CHEMISTRY OF MATERIALS
Article

Chem. Mater. **2010,** *22,* 4919–4930 4919
DOI:10.1021/cm1010345

Selective Deposition of Cobalt Sulfide Nanostructured Thin Films from Single-Source Precursors

Karthik Ramasamy, Mohammad A. Malik, James Raftery, Floriana Tuna, and Paul O'Brien*

The School of Chemistry and The School of Materials, The University of Manchester, Oxford Road, Manchester, M13 9PL, United Kingdom

Received April 14, 2010. Revised Manuscript Received June 10, 2010

The cobalt(III) complexes of 1,1,5,5-tetramethyl- and 1,1,5,5-tetraethyl-2,4-dithiobiuret and the cobalt(II) complex of 1,1,5,5-tetra-*iso*-propyl-2-thiobiuret have been synthesized. The single-crystal X-ray structure of the thiocyanide (**1**) and cobalt tetrachlorate (**2**) salts of the parent cyclized ligand, together with complexes $[Co\{N(SCNMe_2)_2\}_3]$ (**3**), $[Co\{N(SCNEt_2)_2\}_3]$ (**4**) and $[Co\{N(SOCN^iPr_2)_2\}_2]$ (**5**) have been determined. The thermal decomposition of **3**, **4**, and **5** was studied. The complexes were used as single source precursors for the deposition of cobalt sulfide thin films by aerosol assisted chemical vapor deposition (AACVD). The X-ray diffraction (XRD) of the deposited films showed hexagonal $Co_{1-x}S$ from complexes (**3**) and (**4**) whereas complex (**5**) gave a mixture of cubic and hexagonal Co_4S_3. The morphology of films was characterized by scanning electron microscope (SEM) and showed rod like crystallites from **3**, granular crystallites from **4** and stalagmitic structures from **5**. Transmission electron microscopy (TEM) of the samples obtained from thin films from **3** and **4** show that the films are composed of hexagonal nanoplates with nanocubes from **5**. Magnetic measurements showed the para or ferro-magnetic behavior from crystallites. The mechanism for decomposition of precursors to the cobalt sulfide was studied by pyrolysis gas chromatography (Py-GC-MS).

Introduction

Magnetic semiconductors especially cobalt sulfides, have attracted considerable attention in recent years as solar energy absorbers,[1] ultra high-density magnetic recording,[2] anodes for Li-ion batteries,[3] and catalysts for hydrodesulfurization or dehydrodearomatization.[4,5] Cobalt sulfide exists as various crystalline phases: Co_4S_3, Co_9S_8, CoS, $Co_{1-x}S$, Co_3S_4, Co_2S_3, and CoS_2.[6,7] Considerable effort has been focused on depositing cobalt sulfide thin films by various methods such as chemical bath deposition (CBD),[8] chemical vapor deposition (CVD),[9] electrochemical deposition (ECD),[3] and Langmuir–Blodgett (LB)[10] methods. Previously, we have studied methyl n-hexyl dithiocarbamates $[Co(S_2CNMe^nHex)_3]$ as single source precursor for the growth of cobalt sulfide films and reported the deposition of $Co_{1-x}S$, CoS_2 and Co_3S_4.[11] Recently, Co_9S_8 thin films have been deposited by AACVD using iminobisthiophosphinates of cobalt as single source precursor.[12] More recently we have reported synthesis of $Co_{1-x}S$ and Co_4S_3 nanoparticles using thio- and dithio- biuret cobalt complexes.[13,14] To the best of our knowledge no other cobalt complexes have been used as single source precursors for the phase selective deposition of cobalt sulfide thin films. Herein we report the synthesis and structures of ligands **1** and **2** and their cobalt complexes **3**, **4**, and **5**, and their use as single-source precursors for phase selective deposition of $Co_{1-x}S$ and Co_4S_3 thin films by the AACVD method.

Experimental Section

All preparations were performed under an inert atmosphere of dry nitrogen using standard Schlenk techniques. AR reagents were purchased from Sigma-Aldrich chemical company and used as received. Solvents were distilled prior to use. Mass spectra were recorded on a Kratos concept 1S instrument. Infrared spectra were recorded on a Specac single reflectance ATR instrument (4000−400 cm^{-1}, resolution 4 cm^{-1}). Elemental

*Corresponding author. E-mail: paul.obrien@manchester.ac.uk.

(1) Smith, G. B.; Ignatiev, A.; Zajac, G. *J. Appl. Phys.* **1980**, *51*, 4186.
(2) Whitney, T. M.; Jiang, J. S.; Searson, P.; Chien, C. *Science* **1993**, *261*, 1316.
(3) Yue, G. H.; Yan, P. X.; Fan, X. Y.; Wang, M. X.; Qu, D. M.; Wu, Z. G.; Li, C.; Yan, D. *Electrochem. Solid-State Lett.* **2007**, *10*, D29.
(4) Feng, Y. G.; He, T.; Alonso-Vante, N. *Chem. Mater.* **2008**, *20*, 26.
(5) Chen, X. Y.; Zhang, Z. J.; Qiu., Z. G.; Shi., C. W.; Li, X. L. *J. Colloid Interface Sci.* **2007**, *308*, 271.
(6) Wold, A.; Dwight, K. *Solid State Chemistry*; Chapman and Hall.: New York, 1993.
(7) Rao, C. N. R.; Pisharody, K. P. R . *Prog. Solid State Chem.* **1976**, *10*, 207.
(8) Yu, Z.; Du, J.; Guo, S.; Zhang, J.; Matsumoto, Y. *Thin Solid Films.* **2002**, *415*, 173.
(9) Ge., J.; Li *Chem. Commun.* **2003**, 2498.
(10) Luo, X.; Zhang, Z.; Liang, Y *Langmuir* **1994**, *10*, 3213.
(11) Srouji, F.; Afzaal, M.; Waters, J.; O'Brien, P. *Chem. Vap. Deposition* **2005**, *11*, 91.
(12) Paneerselvam, A. PhD Thesis, submitted to the University of Manchester, Manchester, U.K., 2008.
(13) Ramasamy, K.; Maneerprakron, W.; Malik, M. A.; O'Brien, P. Philos. Trans. R. Soc. London, Ser. A. **2010**, DOI:10.1098/rsta.2010.0125.
(14) Ramasamy, K.; Malik, M. A.; O'Brien, P.; Raftery, J. *Dalton Trans.* **2010**, *39*, 1460.

Published on Web 08/04/2010

analysis was performed by The University of Manchester microanalytical laboratory. TGA measurements were carried out by a Seiko SSC/S200 model under a heating rate of 10 °C min^{-1} under nitrogen.

Synthesis of [N(SCNMe$_2$)$_2$]SCN (1). A mixture of dimethylthiocarbamoyl chloride (1.23 g, 10 mmol) and sodium thiocyanate (0.81 g, 10 mmol) in acetonitrile (40 mL) was refluxed with continuous stirring for 1 h, during which time a fine precipitate of sodium chloride formed. To the cooled reaction mixture was added 60% aqueous dimethylamine (1.49 mL, 20 mmol) followed by stirring for 30 min. The mixture was left at room temperature to give colorless needles of the product. Yield 0.72 g (37.8%), MS (EI/CI) major fragments: m/z = [M+] 190, [N(SCNMe$_2$)$_2$] 190. ^{1}H NMR (300 MHz; $CDCl_3$; Me_4Si): 2.3 (s, 6 H). Elemental anal. Calcd for [$C_7H_{12}N_4S_3$]: C, 33.8; H, 4.8; N, 22.5; S, 38.7%. Found: C, 33.2; H, 4.9; N, 21.7; S, 37.8%

Synthesis of [Co{N(SCNMe$_2$)$_2$}$_3$] (3). A solution of dimethylthiocarbamoyl chloride (1.23 g, 10 mmol) and sodium thiocyanate (0.81 g, 10 mmol) in acetonitrile (40 mL) was heated at reflux with continuous stirring for 1 h, during which time a fine precipitate of sodium chloride formed. To the cooled reaction mixture was added 60% aqueous dimethylamine (1.49 mL, 20 mmol) followed by stirring for 30 min and addition of cobalt chloride hexahydrate (1.193 g, 5 mmol). The crude product was precipitated as red powder and recrystallized from chloroform and then by tetrahydrofuran to get suitable quality crystals for X-ray crystallography. Yield 1.89 g (30%), MS (APCI) major fragments: m/z = [M+] 631, [Co{N(SCNMe$_2$)$_2$}$_3$] 631, [N(SCNMe$_2$)$_2$] 190. IR (ν_{max} cm^{-1}): 2928(w), 1468(s), 1380(m), 1306(s), 1104(s), 906(s). Elemental anal. Calcd for $C_{18}H_{36}N_9S_6Co$: C, 34.1; H, 6.1; N, 19.9; S, 30.3; Co, 9.3%. Found: C, 34.9; H, 6.0; N, 19.7; S, 28.9; Co, 9.1%.

Synthesis of [Co{N(SCNEt$_2$)$_2$}$_3$] (4). Compound (**4**) was synthesized by the same method as described for (**3**) but using diethylthiocarbamoyl chloride (1.51 g, 10 mmol) and diethylamine (1.91 mL, 20 mmol). The crude product was precipitated as a black crystalline powder and recrystallized from chloroform to give black needles. Yield 1.90 g (25%), MS (APCI), major fragments: m/z = [M+] 796, [Co{N(SCNEt$_2$)$_2$}$_3$] 796, [N(SCNMe$_2$)$_2$] 246. IR (ν_{max} /cm^{-1}): 2971(w), 2924(w), 1473(s), 1422(s), 1403(m), 1341(s), 1247(s), 1116(s), 996(s). Elemental anal. Calcd for $C_{30}H_{60}N_9S_6Co$: C, 45.2; H, 7.5; N, 15.8; S, 24.0; Co, 7.3%. Found: C, 44.9; H, 7.5; N, 15.7; S, 23.7; Co, 7.3%.

Synthesis of [Co{N(SOCN^{i}Pr$_2$)$_2$}$_2$] (5). Compound (**5**) was synthesized by the same method as described for (**3**) but using di-*iso*-propylcarbamoyl chloride (1.0 g, 6 mmol) and di-*iso*-propylamine (1.49 mL, 12 mmol). The crude product was precipitated as blue powder and recrystallized from tetrahydrofuran to get shiny crystals of blue needles which were identified as (**5**). Yield 1.89 g (30%), MS (APCI) major fragments: m/z = [M+] 631, [Co{N(SOCN^{i}Pr$_2$)$_2$}$_2$], [NSO(CN-*i*-Pr$_2$)$_2$] 284. IR (ν_{max} /cm^{-1}): 2963(s), 1499(s), 1434(s), 1353(s), 1208(m), 1144(m). Elemental anal. Calcd for $C_{28}H_{56}N_6S_2O_2Co$: C, 53.2; H, 8.8; N, 13.3; S, 10.1; Co, 9.3%. Found: C, 53.2; H, 9.0; N, 13.2; S, 9.9; Co, 9.0%

X-ray Crystallography. Single-crystal X-ray diffraction data for the compounds were collected using graphite monochromated Mo−Kα radiation (λ = 0.71073 Å) on a Bruker APEX diffractometer. The structure was solved by direct methods and refined by full-matrix[15] least-squares on F^2. All non-H atoms were refined anisotropically. H atoms were included in calculated positions, assigned isotropic thermal parameters and allowed to ride on their parent carbon atoms. All calculations were carried out using the SHELXTL package.[16] The details pertaining to the data collection of the crystals are as follows: (**1**) $C_7H_{12}N_4S_3$, M = 248.39, colorless needles, monoclinic, space group $P2(1)/n$, a = 10.409(2) Å, b = 5.863(9) Å, c = 18.465(4) Å, α = 90°, β = 99.965° (4), γ = 90°, volume = 1110.1(3) A^3, Z = 4, D = 1.486 Mg/m^3, T = 100(2) k, reflections collected = 3193/3269, final R indices [$I > 2\sigma(I)$], R1 = 0.0751, wR2 = 0.1779, R indices (all data) = R1 = 0.0835, wR2 = 0.1826, largest diff. peak and hole = 1.674 and −0.994 e A^{-3}, GOF = 1.101. (**2**) $C_{12}H_{24}N_6S_4CoCl_4$, M = 581.34, green needles, orthorhombic, space group $Pca2(1)$, a = 13.978(2) Å, b = 9.226(2) Å, c = 18.155(3) Å, α = 90°, β = 90°, γ = 90°, volume = 2341.3(6) A^3, Z = 4, D = 1.649 Mg/m^3, T = 100(2) k, reflections collected = 13 972/4740, unique reflections = [R(int) = 0.0424], final R indices [I > 2σ(I)] R1 = 0.0354, wR2 = 0.0635, R indices (all data) = R1 = 0.0421, wR2 = 0.0655, largest diff. peak and hole = 0.412 and −0.284 e A^{-3}, GOF = 1.022. (**3**) $C_{18}H_{36}N_9S_6Co$, M = 629.85, black cubes, orthorhombic, space group $Pca2(1)$, a = 14.872(2) Å, b = 13.832(2) Å, c = 13.450(2) Å, α = 90°, β = 90°, γ = 90°, volume = 2767.1(7) A^3, Z = 4, D = 1.512 Mg/m^3, T = 100(2) k, reflections collected = 16 614/6283, unique reflections = [R(int) = 0.0842], final R indices [$I > 2\sigma(I)$] R1 = 0.0432, wR2 = 0.0680, R indices (all data) = R1 = 0.0890, wR2 = 0.0754, largest diff. peak and hole = 0.674 and −0.343 e A^{-3}, GOF = 0.676. (**4**) $C_{30}H_{60}N_9S_6Co$, M = 798.16, black cubes, monoclinic, space group $P2(1)/C$, a = 9.580(8) Å, b = 42.691(4) Å, c = 9.637(8) Å, α = 90°, β = 90°, γ = 90°, Volume = 3908.7(6) A^3, Z = 4, D = 1.356 Mg/m^3, T = 100(2) k, reflections collected = 24 649/9126, unique reflections = [R(int) = 0.0779], final R indices [$I > 2\sigma(I)$] R1 = 0.0599, wR2 = 0.0789, R indices (all data) = R1 = 0.1117, wR2 = 0.0918, Largest diff. peak and hole = 0.632 and −0.623 e A^{-3}, GOF = 0.891. (**5**) $C_{28}H_{56}N_6O_2S_2Co$; M = 631.84; blue needles; monoclinic; $C2/c$; a = 14.435(5) Å, b = 18.350(6) Å, c = 25.972(8) Å; β = 91.433(6)°; V = 6877(4) $Å^3$; Z = 8; D = 1.220 Mg/m^3; T = 100(2) K; reflections collected = 18076, unique reflections = 4202 [R(int) = 0.1603]; R1 = 0.1052 and wR2 = 0.2104 for [$I > 2\sigma(I)$]; R1 = 0.1424 and wR2 = 0.2261 for all data; largest diff. peak and hole = 0.768 and −0.551 e A^{-3}, GOF = 1.206 CCDC reference numbers 685542, 685539, 692258, 698375, and 715970.

Deposition of Films by AACVD. In a typical experiment, 0.25 mmol of the complex **3**, **4**, or **5** was dissolved in 20 mL of tetrahydrofuran in a two-necked 100 mL round-bottom flask with a gas inlet that allowed the carrier gas (argon) to pass into the solution to aid the transport of the aerosol. This flask was connected to the reactor tube by a piece of reinforced tubing. The argon flow rate was controlled by a Platon flow gauge. Seven glass substrates (approximately 1 × 3 cm) were placed inside the reactor tube, which is placed in a CARBOLITE furnace. The precursor solution in a round-bottom flask was kept in a water bath above the piezoelectric modulator of a PIFCO ultrasonic humidifier (model 1077). The aerosol droplets of the precursor thus generated were transferred into the hot wall zone of the reactor by carrier gas. Both the solvent and the precursor were evaporated and the precursor vapor reached the heated substrate surface where thermally induced reactions and film deposition took place.

Pyrolysis GC-MS. Pyrolysis GC-MS analysis was carried out using a Hewlett-Packard 5890 gas chromatograph linked to a VG Trio-2000 mass spectrometer. The chromatography conditions were as follows: column BP5 (supplied by SGE); bonded phase methyl siloxane, length 25 m, inner diameter 0.22 mm; phase thickness 0.25 μm. The temperature program employed

(15) Sheldrick, G. M. *SHELXS-97 and SHELXL-97*; University of Göttingen: Göttingen, Germany, 1997.

(16) Bruker. *SHELXTL Version 6.12*; Bruker AXS: Madison, WI, 2001.

Scheme 1. Schematic Representation of the Synthesis of Ligand and Complexes

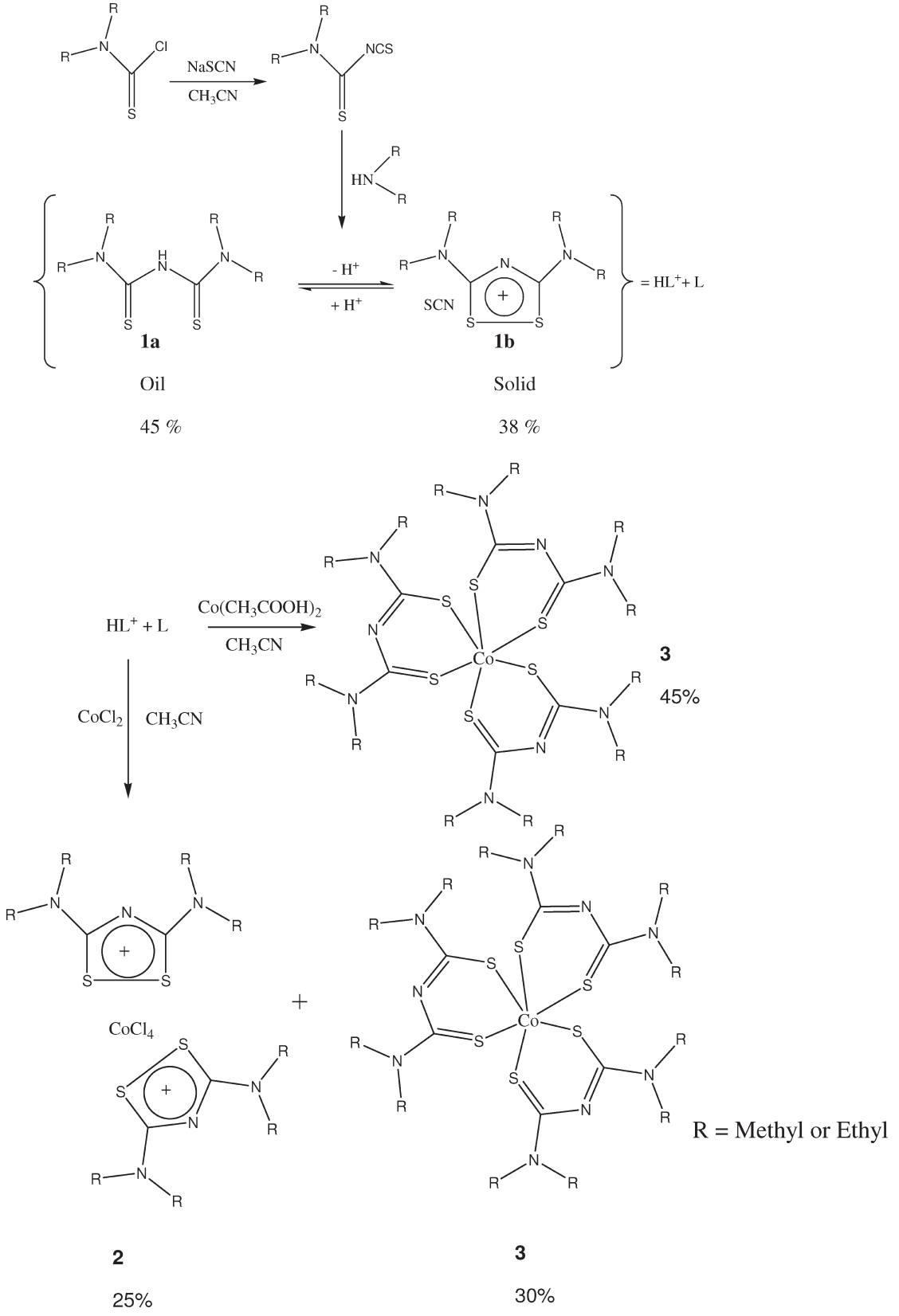

for analysis was; initial temperature 40 °C, initial time 2 min, 8 °C min^{-1} to 300 °C, final time 30 min. The pyrolysis injector temperature was 295 °C. The carrier gas (helium) pressure was kept at 12 psi with flow rate of 1 cm^3 min^{-1}. MS settings were 70 kV electron energy, source temperature 200 °C, 100 μA beam current and 7 kV detector voltage. Mass spectra were recorded between 40 and 800 atomic mass unit with a scan speed of 0.9 s. The complex (<0.1 mg) was packed between the silica gel and sealed in a capillary tube

Characterization of Thin Films. X-ray diffraction studies were performed on a Bruker AXS D8 diffractometer using Cu−Kα

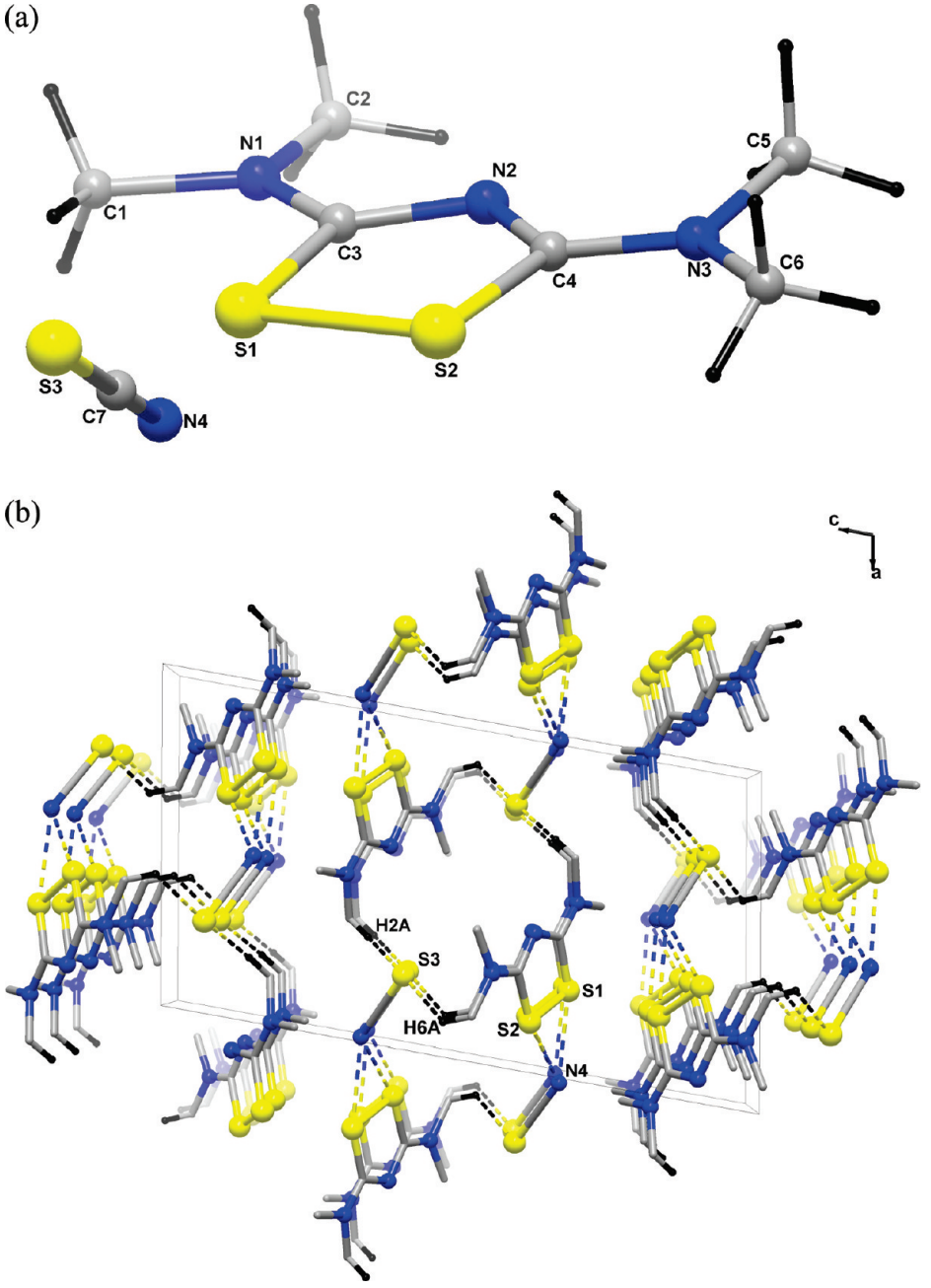

Figure 1. (a) X-ray structure of **1**. Selected bond lengths (Å) and bond angles (deg): C1−N1 1.465(5), C2−N1 1.471(5), C3−S1 1.768(4); N2−C4−S2 120.1(3), C4−S2−S1 92.9(1). (b) View showing the supramolecular network mediated by C−H···S and C−N···S interactions.

radiation. The samples were mounted flat and scanned between 20 to 80° in a step size of 0.05 with a count rate of 9 s. Films were carbon coated using Edward's E306A coating system before carrying out SEM and EDX analyses. SEM analysis was performed using a Philips XL 30FEG and EDX was carried out using a DX4 instrument. TEM analysis was performed using cm200 instrument. High resolution transmission electron microscopy (HRTEM) was performed using Tecnai F30 FEG TEM instrument, operating at 300 kV, all samples deposited over carbon coated copper grids. Selected area electron diffraction (SAED) was performed using a Phillips CM200 microscope at an accelerating voltage of 200 kV. Magnetic measurements were performed in the temperature range 1.8−300 K, by using a Quantum Design MPMS-XL SQUID magnetometer equipped with a 7 T magnet. The diamagnetic corrections for the compounds were estimated using Pascal's constants, and magnetic data were corrected for diamagnetic contributions of the sample holder.

Results and Discussions

The reaction of *N*,*N*′-dimethylthiocarbamoyl chloride, sodium thiocyanate, and dimethylamine produced a cyclized ligand cation stabilized by a thiocyante ion. Addition of cobalt chloride to this reaction gave a mixture of compounds **2** and **3**. Compound **2** was unexpectedly identified as consisting of two cyclized ligand cations stabilized by cobalt tetrachlorate ion, whereas compound **3** was identified as the expected cobalt complex but of cobalt(III). A schematic representation of the reaction is shown in Scheme 1. The cyclization of the ligand as observed in compound **2** had been discussed by Pellacani et al.[17] in dithiomalonamide systems

(17) Menabue, L.; Pellacani, G. C. *J. Chem. Soc., Dalton Trans.* **1976**, 455.

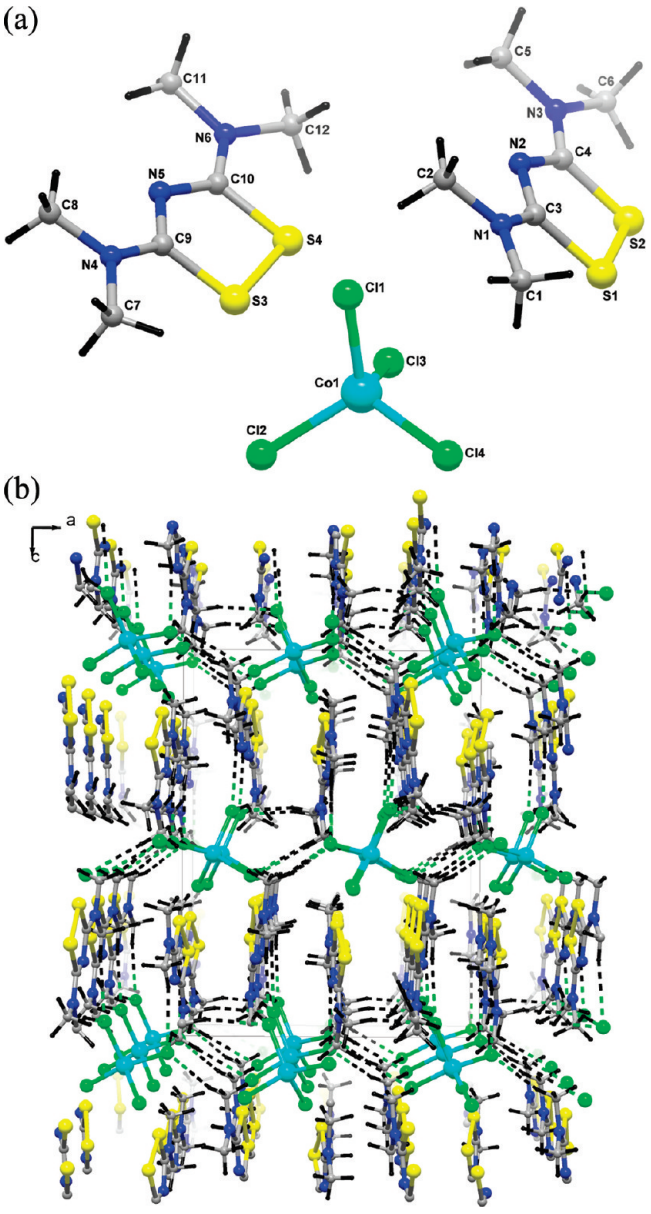

Figure 2. (a) X-ray structure of **2**. Selected bond lengths (Å) and bond angles (deg): C1−N1 1.457(4), C3−S1 1.770(3), S1−S2 2.064(1); N3−C4−N2 122.5(3), Cl4−Co1−Cl1 107.3(4). (b) View showing the supramolecular network mediated by C−H···Cl and Co−Cl···S interactions.

and proposed mechanism for formation of dithiolium salts based on polarographic investigations. Köhler et al.[18] observed the same for dithiazolium tetrachloroniccolate. The reaction of *N*,*N*′-diethylthiocarbamoyl chloride, sodium thiocyanate and neat diethylamine followed same behavior as explained above. All three complexes are air and moisture stable for several months and soluble in most organic solvents (toluene, tetrahydrofuran, chloroform, dichloromethane), which makes them suitable for AACVD.

X-ray Single-Crystal Structure of [N(SCNMe$_2$)$_2$]SCN (1). The X-ray single-crystal structure shows a planar five-membered disulfide ring with bite angles of N(2)C(4)S(2)−120.1(3)° and C(4)N(2)C(3)−114.6(4)°, which are slightly smaller than for trigonal planar. The bond lengths of C(4)−S(2) 1.758(4) and S(1)−S(2) 2.0568(15) indicate partial charge delocalization over the atoms.

(18) Köhler, R.; Sieler, J.; Richter, R.; Hoyer, E.; Beyer, L. *Z. Anorg. Allg. Chem.* **1989**, *576*, 203.

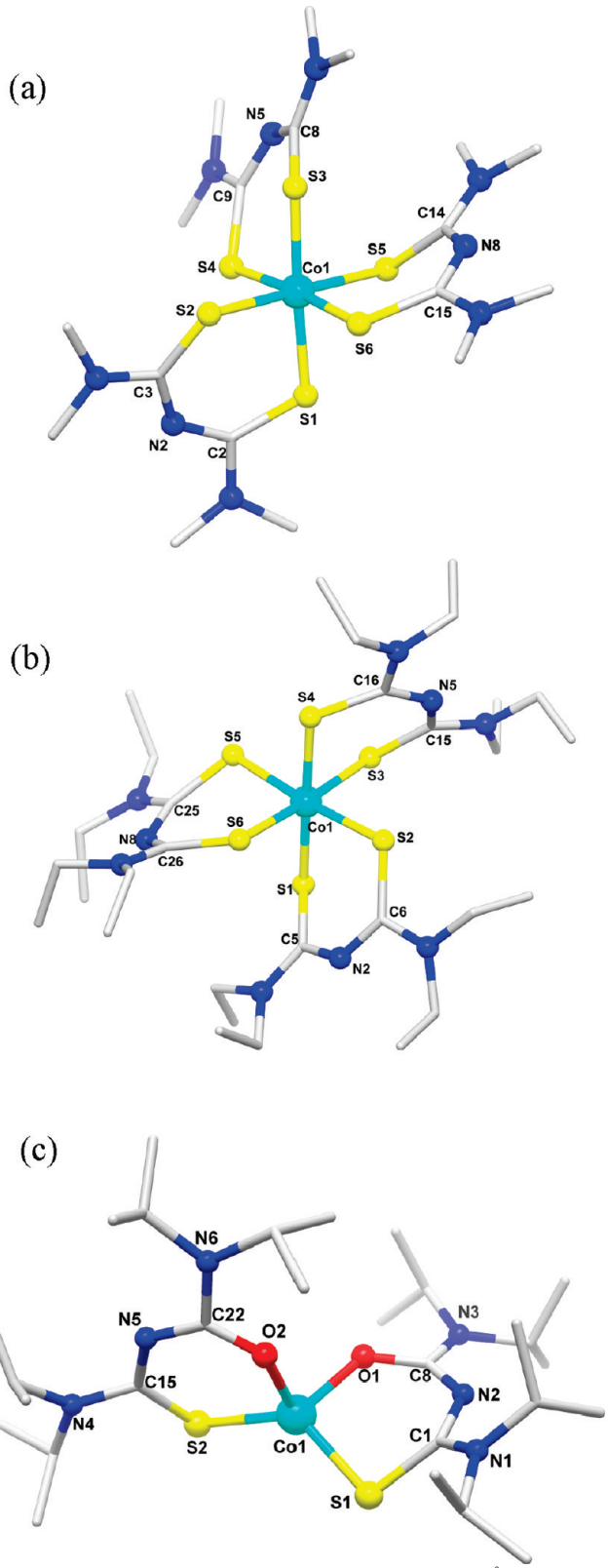

Figure 3. (a) X-ray structure of **3**. Selected bond lengths (Å) and bond angles (deg): C1−N1 1.458(6), C2−S1 1.723(5), Co1−S4 2.231(1); C2−N2−C3 127.7(5), S4−Co1−S3 94.3(6). (b) X-ray structure of (**4**). Selected bond lengths (Å) and bond angles (deg) C1−N1 1.454(4), C6−S2 1.723(4), C16−S4 1.737(4); N2−C5−S1 127.9(3), S2−Co1−S1 91.7(4). (c) (a) X-ray structures of (**5**). Selected bond lengths (Å) and bond angles (deg): Co(1)−O(1) 1.918 (7), Co(1)−S(2) 2.149, N(2)−C(8) 1.261(1), N-(2)−C(1) 1.336(1); O(1)−Co(1)−S(1) 96.7 (2), C(8)−N(2)−C(1) 124.2 (1).

Structure refinement data are given in the Experimental Section, selected bond angles, and bond distances are given in the caption to Figure 1. The crystal packing diagram in Figure 1b shows weak interactions between thiocyanide and sulur in the range 2.935−3.022 Å, which gives a supramolecular chainlike network by linking each thiocyanide ion with two molecules of cyclized ligand cation.

X-ray Single-Crystal Structure of $[N(SCNMe_2)_2]_2CoCl_4$ (2). The X-ray single-crystal structure shown in Figure 2a shows a tetrahedral geometry of cobalt. The ligand bite angles of 109.68(4) and 111.29(4)° are somewhat larger than perfect tetrahedral coordination. Weak interactions connect the cyclized ligand through the sulfur atom with $[CoCl_4]^{2-}$ by 3.221−3.531 Å distance another unit of ligand cation connects $CoCl_4^{2-}$ unit by 2.930 Å through methyl hydrogen of dimethylamine. Structure refinement data are given in the experimental section, selected bond angles and bond distances are given in caption to Figure 2. The crystal packing diagram in Figure 2b shows weak interactions that give a double packed chain network and each $[CoCl_4]^{2-}$ unit connects four units of the ligand cation.

X-ray Single-Crystal Structure of $[Co\{N(SCNMe_2)_2\}_3]$ (3). The X-ray single-crystal structure of $[Co\{N(SCNMe_2)_2\}_3]$ (**3**) (Figure 3a) shows cobalt in an octahedral geometry with the ligand bite angles of 93.98(6), 94.29(6), and 94.34(6)°, which are slightly larger than those for perfect square planar configuration. The bond lengths between C(2)−S(3) 1.718(5) are lower than for the cyclized ligand 1.758(4), which may be due to partial delocalization of positive charge over the atoms in cyclized ligand. Structure refinement data are given in the Experimental Section and selected bond angles and bond lengths are given in caption to Figure 3a.

X-ray Single-Crystal Structure of $[Co\{N(SCNEt_2)_2\}_3]$ (4). The X-ray single crystal structure of $[Co\{N(SCNEt_2)_2\}_3]$ (**4**) in (Figure 3b) shows cobalt in octahedral geometry with the ligand bite angles of 93.37(4), 92.58(4), and 91.73(4)°. The separations C(5)−S(1) 1.734(4) are intermediate between the values found for cyclized ligand 1.758(4) and complex (**3**) 1.718(5), which may be due to stronger electron donating nature of diethyl amine. Structure refinement data are given in the Experimental Section, and selected bond angles and bond lengths are given in the caption for Figure 3b.

X-ray Single-Crystal Structure of $[Co\{N(SOCN^iPr_2)_2\}_2]$ (5). The X-ray single-crystal structure of $[Co\{N(SOCN^iPr_2)_2\}_2]$ (**5**) shows cobalt(II) ion is tetrahedral with an S_2O_2 donor set. Within each of the two thiobiuret ligands, the four atoms of the urea or thiourea groups are close to being coplanar. However, overall, the two thiobiuret ligands all show significant deviation from planarity because of twisting about the central N atom; the dihedral angles between the two pairs of urea and

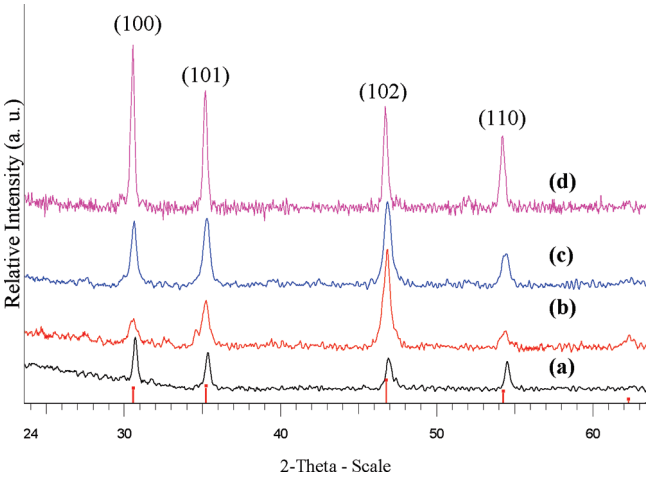

Figure 4. XRD pattern of CoS films deposited on glass at (a) 350, (b) 400, (c) 450, and (d) 500 °C from **3**. Solid lines are for hexagonal $Co_{1-x}S$ (ICDD-042−0826).

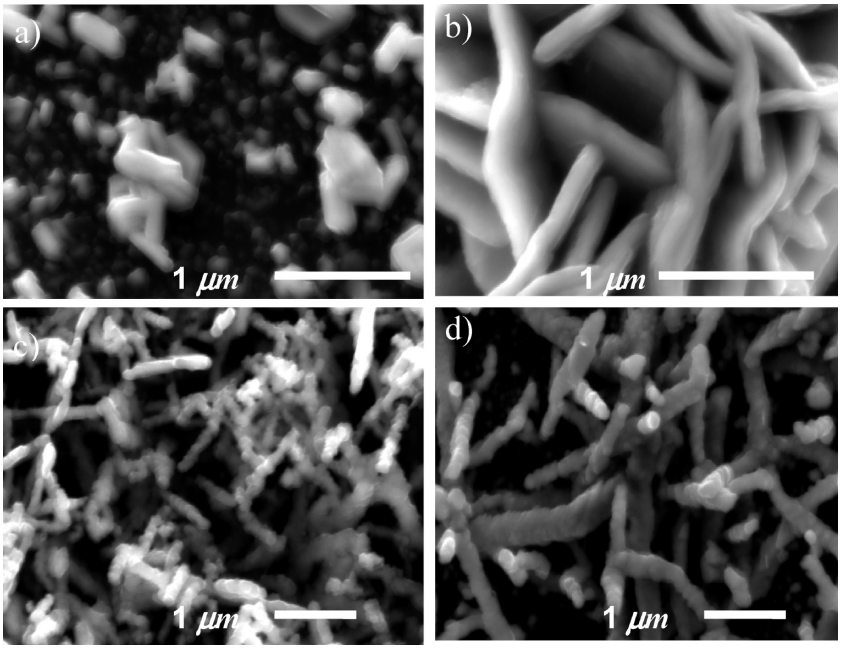

Figure 5. SEM images of films deposited from **3** on glass at (a) 350, (b) 400, (c) 450, and (d) 500 °C.

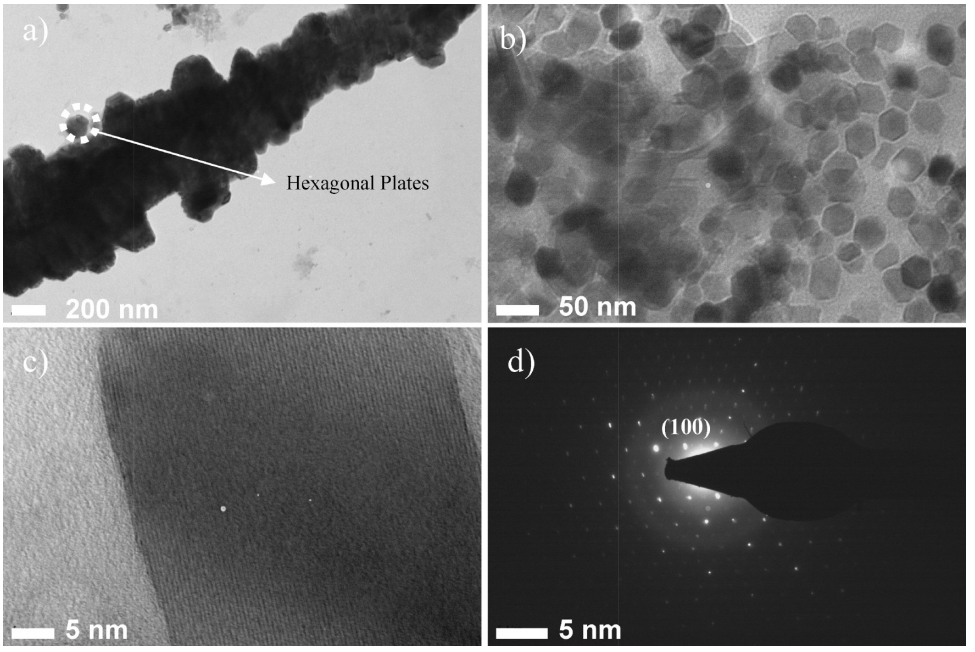

Figure 6. (a, b) Low- and high-magnification TEM images of films deposited on glass at 500 °C, (c) HRTEM image, (d) SAED pattern from **3**.

thiourea are 124.2(1) and 122.5(2)°. In both ligands, the pattern of bond distances indicates that the formal negative charge is predominately localized on the S atom. The relatively long C−S and short C−O average bond lengths of 1.749(1) and 1.300(2) Å are consistent with mostly single and double bond character, respectively, and this bond localization is also reflected in the average C−N bond distances to the central N atom: 1.336(2) Å in the (iso)-thiourea group and 1.261(2) Å in the urea group. One of the ligands is disordered and has been modeled on a ratio of 47:53. Structure refinement listed in the Experimental Section. Selected bond angles and bond lengths are listed in caption for Figure 3c.

Thermogravimetric Analysis. Thermogravimetric analysis of complexes **3**, **4**, and **5** show that the complexes decomposed in a single step between 228 and 320, 210−329 and 140−230 °C, respectively, with the observed final residue of 20.0% for complex **3** in good agreement with the calculated 19.5% for cobalt disulfide. The observed final residue 14.5% for complex **4** is close to the calculated 15.4% for cobalt disulfide and from complex **5** also observed final residue of 18.0% is close to the calculated value of 19.5% for cobalt disulfide

Deposition of Thin Films. *$Co_{1-x}S$ Films from* [*Co*{*N*-(*SCNMe*$_2$)$_2$}$_3$] (***3***). Film deposition was carried out at substrate temperature from 350 to 500 °C with argon flow rate at of 160 sccm. No deposition was obtained below 350 °C. Films deposited at 350 or 400 °C were black in color, not uniform, but adherent, whereas reflective black films were deposited at 450 or 500 °C. XRD pattern of as deposited films at 350−500 °C (Figure 4) show formation of cobalt sulfide films indexed to NiAs type- hexagonal phase of $Co_{1-x}S$. No characteristic XRD peaks arising from possible impurities are detected. The intensity of the peaks increased with increasing deposition temperature. This observation suggests the formation of bigger crystallites at higher temperatures.

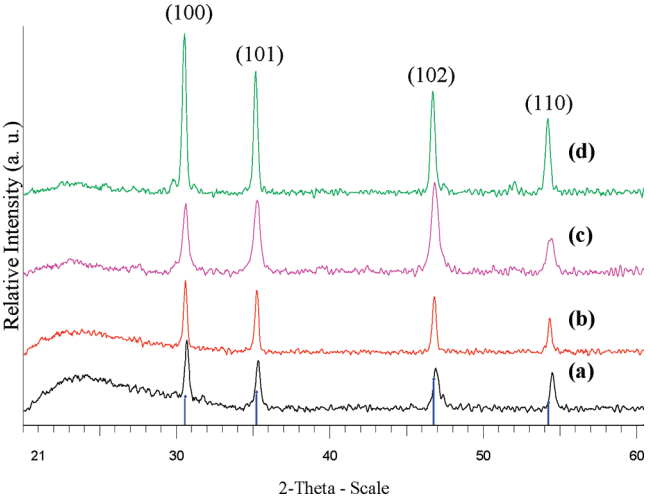

Figure 7. XRD pattern of CoS films deposited from **4** on glass at (a) 350,(b) 400, (c) 450, and (d) 500 °C. Solid lines are for hexagonal $Co_{1-x}S$ (ICDD-042−0826).

The dominant peaks can be assigned to the (100), (101), (102), and (110) reflections of hexagonal $Co_{1-x}S$ as shown in Figure 4. The SEM images of the films (Figure 5) show that the morphology of the cobalt sulfide is depends on the growth temperature. The as deposited films at 350 °C consist of granular crystallites and rods, whereas at higher temperatures of 450 or 500 °C showed only rods. The diameter of the rods increased from 200 to 500 nm as the deposition temperature was increased from 450 to 500 °C. EDX analysis show composition of the films as cobalt: sulfur 55:45 (350 or 400 °C, 53 47 (450 °C) and 54:46 (500 °C).

The TEM image in Figure 6 showed rods composed of hexagonal nanoplates. The size of the nanoplates ranged from ca. 25 to 30 nm as shown in Figure 6b. The single hexagonal nanoplates have tendency to serve as the primal structure to form the secondary microrod structures.

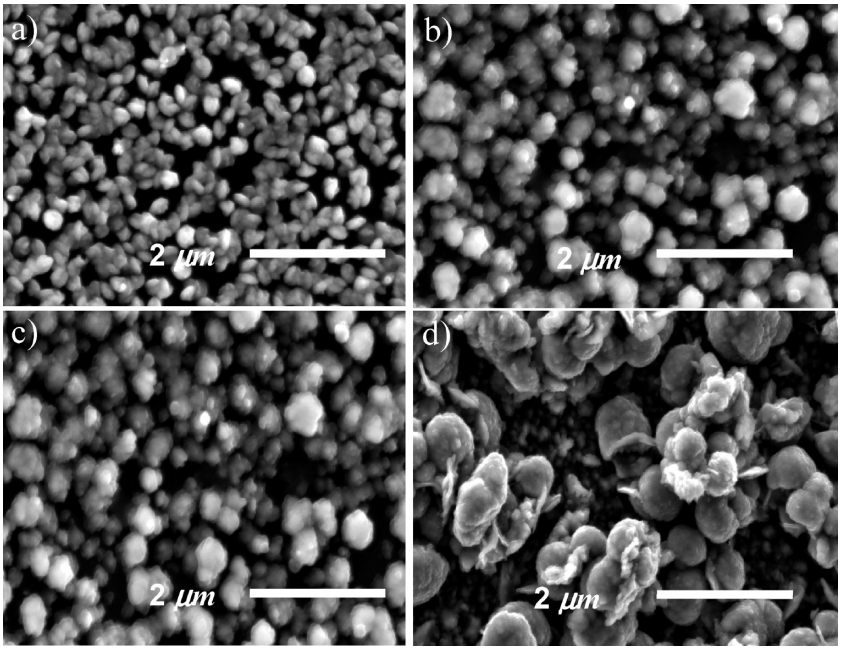

Figure 8. SEM images of films deposited from **4** on glass at (a) 350, (b) 400, (c) 450, and (d) 500 °C.

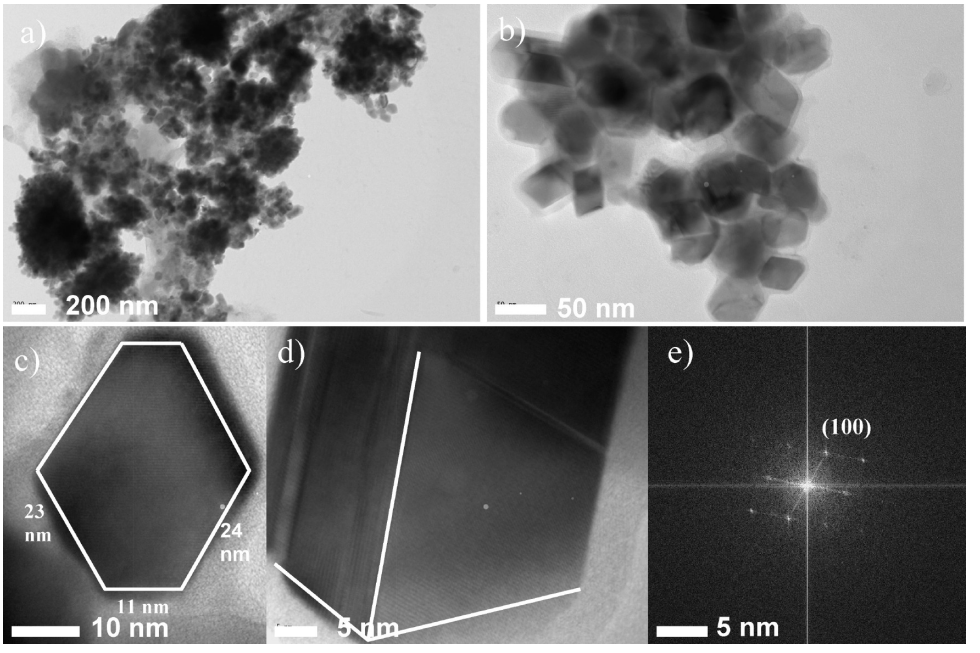

Figure 9. (a, b) Low- and high-magnification TEM images of films deposited on glass at 500 °C, (c, d) HRTEM images, (e) SAED pattern from **4**.

The driving force for the formation of microrods by oriented attachment mechanism has been reported as reduction in overall surface energy,[19] which can be realized by eliminating the surface at which the crystallites join.

The proposed crystal growth mechanism has been described in work on ZnO,[20] TiO_2,[21] CuO,[22] ZnS,[23] and CuS.[24] In this way, oriented attached CoS will further attach to eliminate the surface and form the secondary structure. Figure 6a clearly shows the sidewise attachment of hexagonal nanoplates stacked together to form microsized rods. The SAED pattern in Figure 6d shows the single-crystalline nature of nanoplates. The diffraction spot can be indexed to the (100) plane of the hexagonal phase.

$Co_{1-x}S$ Films from [$Co\{N(SCNEt_2)_2\}_3$] (***4***). Film deposition was carried out at substrate temperature from 350 − 500 °C with argon flow rate of 160 sccm. No films deposition occurred below 350 °C. Black adherent films obtained at the higher temperatures. The XRD patterns

(19) Penn, R. L.; Banfield, J. F. *Geochim, Cosmochim. Acta*. **1999**, *63*, 1549.
(20) Liu, B.; Zeng, H. C. *J. Am. Chem. Soc*. **2003**, *125*, 4430.
(21) Chemseddine, A.; Moritz, T. *Eur. J. Inorg. Chem*. **1999**, 235.
(22) Zhang, Z. P; Sun, H. P.; Shao, X. Q.; Li, D. F.; Yu, H. D.; Han, M. Y. *Adv. Mater*. **2005**, *17*, 42.
(23) Huang, F.; Zhang, H. Z.; Banfield, J. F. *J. Phys. Chem. B* **2003**, *107*, 10470.
(24) Xu, H.; Wang, W.; Zhu, W. *Chem. Lett*. **2006**, *35*, 264.

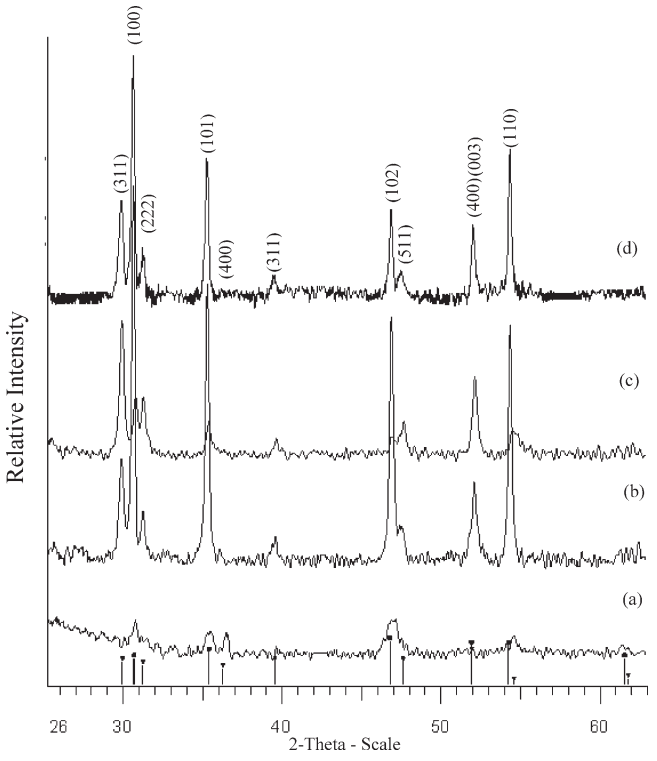

Figure 10. XRD pattern of Cobalt sulfide films deposited on glass at (a) 280, (b) 320, (c) 360, and (d) 400 °C from (**5**). Symbols ▼ indicating cubic (ICDD-02-1338) and ■ indicating hexagonal (ICDD-02-1458) Co_4S_3 phases.

of the as deposited films at 350 - 500 °C show formation of polycrystalline cobalt sulfide films which could be indexed to NiAs type-hexagonal phase of $Co_{1-x}S$ (Figure 7). Higher intensities peaks were obtained for the films deposited at 450 or 500 °C. The dominant peaks can be assigned the CoS (100), (101), (102), and (110) reflections of hexagonal $Co_{1-x}S$ as like with the films grown from complex **3**.

The SEM images in Figure 8 show that the growth of smaller individual granular crystallites (size 300−350 nm) at 350 and 400 °C, whereas granular clusters (size 450−500 nm) were formed in the films grown at 450 °C. Films deposited at 500 °C showed a flower like morphology (size 1−1.5 μm). EDX analysis shows that the films are composed of cobalt:sulfur 55:45 (350 °C), 53:47 (400 °C), and 54:46 (450 and 500 °C). The Co:S ratio is closer to 1:1 in the films deposited at temperatures higher than 350 °C.

The TEM images (Figure 9) of the samples from thin films grown at 500 °C showed flower like crystallites composed of hexagonal nanoplates and nanocubes size range from 30 to 35 nm. The growth of flower like shape differs from with complex (**3**) and may reflect imperfect oriented attachment growth of nanoplates it is well-known that the oriented attachment not constrained to single structure. The only requirement is that the surface of the attaching particles be dimensionally similar.[25]

The formation of dislocations at bonding interface of may be driving force for formation of imperfect oriented attachment The SAED pattern in Figure 9(e) shows single crystalline nature of nanoplates. The diffraction spot can be indexed to the (100) plane of the hexagonal phase. Complex **3** is structural similar to complex **4** with an ethyl substituted rather than methyl. Thermo gravimetric analysis of both complexes **3** and **4** gave residues of CoS_2. The XRD pattern of thin films deposited from both complexes **3** and **4** show the same phase ($Co_{1-x}S$) but differing in morphology.

Co_4S_3 Films from [$Co\{N(SOCN^iPr_2)_2\}_2$] (**5**). Film deposition was carried out at substrate temperature from 280 to 400 °C with an argon flow rate of 160 sccm. No deposition was obtained below 280 °C. Black adherent films were deposited at 280 and 320 °C, whereas uniform reflective black films were deposited at 360 and 400 °C. The XRD pattern of as deposited films at 280−400 °C (Figure.10) shows the formation of mixed phase cobalt sulfide indexed to cubic and hexagonal phase of Co_4S_3. No characteristic XRD peaks arising from possible impurities are detected. The X-ray diffractions peaks of films deposited at 280 °C show almost same intensities of cubic and hexagonal phase. At higher temperature, hexagonal peaks are dominant. This shows formation of bigger hexagonal crystallites at higher temperatures. The XRD peaks can be assigned to the cobalt sulfide (100), (101), (102), and (110) reflections of hexagonal and (311), (222), (400), (331), (511), and (440) of cubic Co_4S_3 as shown in Figure. 10.

The SEM images of the films (Figure 11) show that the morphology of the cobalt sulfide is dependent on the growth temperature. Films deposited at 280 °C consist of spherical crystallites with an average size of 250 nm and films at 320 °C show the growth of cuboids. The same images from higher temperature films 360 or 400 °C show as tree like crystallites similar to stalagmite structures growing in the *z*-direction which probably is due to stacking of the many smaller crystallites. EDX analysis show composition of the films as cobalt: sulfur 60:40 (280 and 320 °C), 61:39 (360 °C) and 62:38 (400 °C). The TEM images of the ground crystallites from the films grown at 400 °C show nanocubes of the size ranging from ca. 25 to 30 nm as shown in Figure 12a.

HRTEM images of the nanocube (Figure. 12b and c) shows the lattice fringes with a *d*-spacing 0.292 nm corresponding to (100) reflection of hexagonal Co_4S_3 and 0.299 nm corresponding to (311) reflection of cubic Co_4S_3. The single nanocubes have tendency to serve as the primal structure to form the secondary microcuboids structure. The SAED pattern in Figure 12d shows the single-crystalline nature of nanoplates. The diffraction spot can be indexed to the (100) plane of the hexagonal phase.

Mechanistic Studies by Py-GC-MS. Pyrolysis GC-MS is a useful technique to identify the decomposition behavior of the metal organic complexes.[26] We were able to propose the possible decomposition path ways from the relatively stable charged fragments observed in GC-MS. In Scheme 2, a plausible decomposition mechanism is

(25) Penn, R. L.; Banfield, J. F. *Science* **1998**, *281*, 969.

(26) Chunggaze, M.; Malik, M. A.; O'Brien, P. *J. Mater. Chem.* **1991**, *9*, 2433.

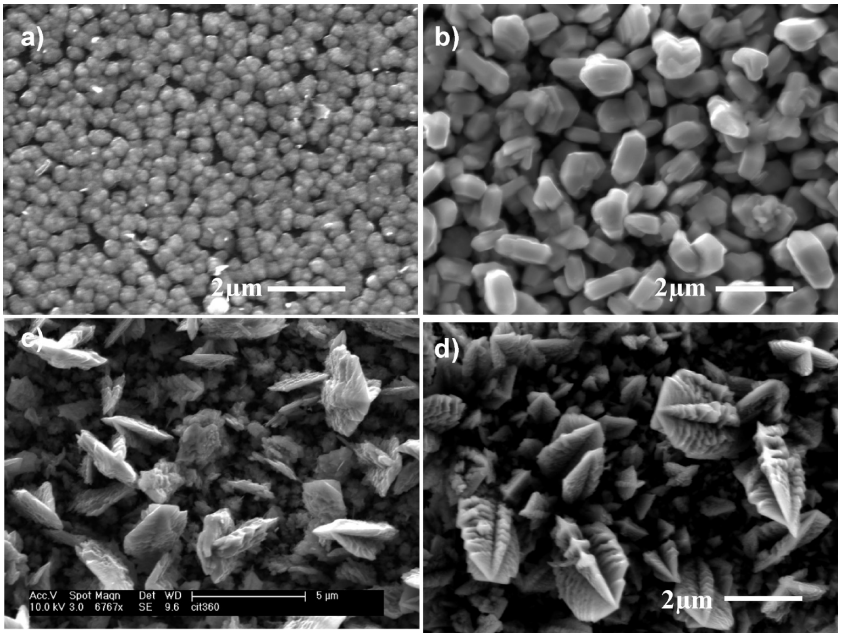

Figure 11. SEM images of films deposited on glass at (a) 280, (b) 320, (c) 360, and (d) 400 °C from $[Co\{N(SOCN^iPr_2)_2\}_2]$ (**5**).

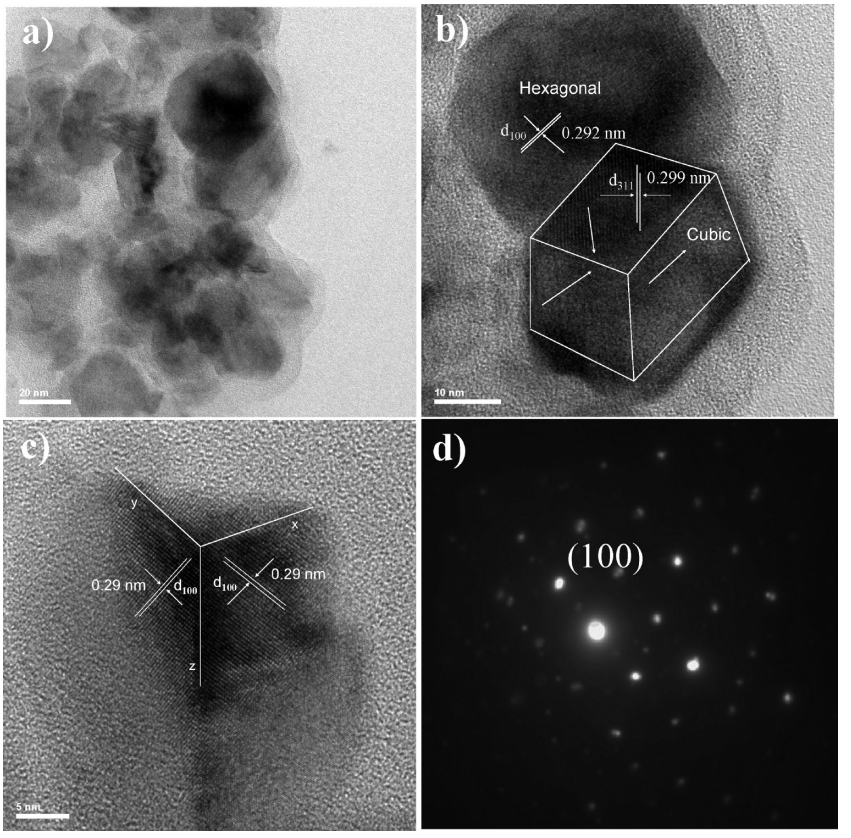

Figure 12. (a) TEM images of cobalt sulfide films deposited from (**5**) on glass at 400 °C, (b, c) HRTEM images, (d) SAED pattern.

presented for the complexes **3**, **4**, and **5**, summarizing the main intermediates and products. Each intermediate species can be rationalized through the observation of a corresponding fragment in the pyrolysis MS experiment and each species in Scheme 2 is presented with the m/z value corresponding to the fragment, if observed in one of the GC-MS experiments. The proposed mechanism involves common decomposition steps for complexes **3** and **4**, whereas for complex **5**, a slightly different pathway leads to the cobalt sulfides. In the first step, the elimination of the dialkylamine occurs with the observed m/z value of 42 (**3**) and 73 (**4**), leading to the formation of common deaminated intermediate **A** for complexes **3** and **4**. The second step involves the reductive elimination of thiazolium group with the predominant m/z value of 102 for complexes **3** and **4**, which is not observed for com-

Scheme 2. Plausible Decomposition Mechanism for (3), (4) and (5) from Pyrolysis GC-MS Studies.

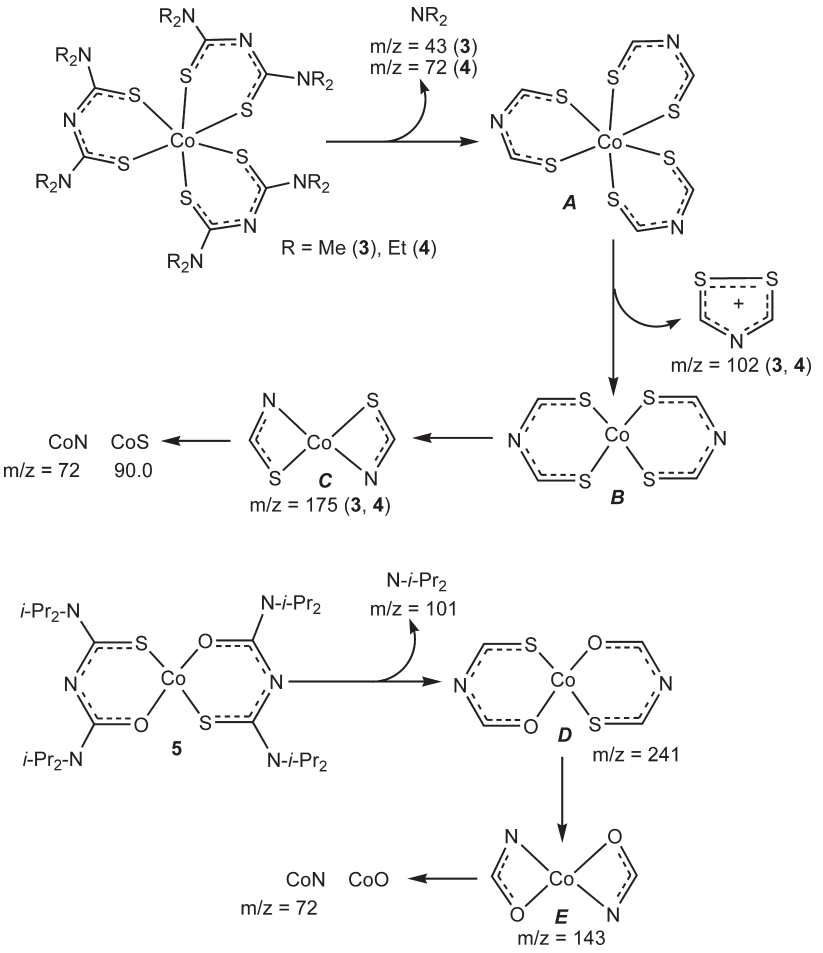

plex **5**. Followed by elimination of −CS group leading to bidentate S, N-donated cobalt complex **C** with a stable peak at 175 leading to the formation of cobalt sulfide (90.0). Complex **5** also follows the similar decomposition in first step which involves the elimination of di-*iso*-propylamine with an observed mass value of 101. In second step cleavage of Co−S bond occurs instead of Co−O bond leading to the formation of intermediate **E.** The most significant aspect of formation of intermediate **E** can be explained by the little observable difference in the bond lengths Co−O 1.918, Co(1)−S(2) 2.149; therefore, Co−S bonds are likely to be weaker. So, the fragmentation would most likely result in preferential dissociation of the Co−S bond, ultimately resulting in the formation of intermediate **E** with an observed mass of 143. The decomposition of **E** leads to the formation of CoO or CoN (72), which is in contrast to the results obtained from AACVD showing the deposition of cobalt sulfide films without any nitride or oxide impurities. This observation also shows that the GC/MS pyrolysis does not exactly provide the conditions under which a AACVD experiment works, although it gives us some clues to the decomposition pathways leading to the final product.

Magnetic Measurement of Cobalt Sulfide Thin Films. The electrons in cobalt sulfide occupy in partially filled d-subshells. From the magnetic measurement, it should be possible to evaluate phase relationships that exist in cobalt sulfide systems. DC magnetization plot of $Co_{1-x}S$ thin films deposited on GaAs substrate at 400 °C from complex **3** is shown in Figure 13a. Magnetization versus temperature for ZFC and FC experiments at 1-kOe magnetic fields are given in Figure 13a. It shows that the ZFC and FC magnetization curves superimpose to each other and increase with decreasing temperature, which indicates the paramagnetic behaviour of $Co_{1-x}S$ crystallites. The same paramagnetic nature was observed for the films deposited from complex **4**. This result is in good agreement with the literature report for the same phase of nanoparticles,[27] whereas films of Co_4S_3 phase deposited from complex **5** showed ferromagnetic behavior. Heidelberg et al.[28] investigated the magnetic properties of various phases of cobalt sulfur system and reported the composition region of Co_4S_3 were ferromagnetic below 1070 K. Magnetization versus field curves shows no measurable magnetization at 300 K. However on decreasing the temperature to 5 K, the increase in magnetization linearly observed as peculiar for paramagnetic substances with the highest magnetization value of 23.2 emu/g for the $Co_{1-x}S$ films deposited from complex **3** (Figure 13a, inset). 31.7 emu/g for the $Co_{1-x}S$ films deposited from complex **4**

(27) Dutta, D. P.; Sharma, G.; Gopalakrishnan, I. K. *Mater. Lett.* **2008**, *62*, 1275.
(28) Heidelburg, H. F.; Luxem, A. H.; Talhouk, S.; Banewicz, J. J. *Inorg. Chem.* **1966**, *5*, 194.

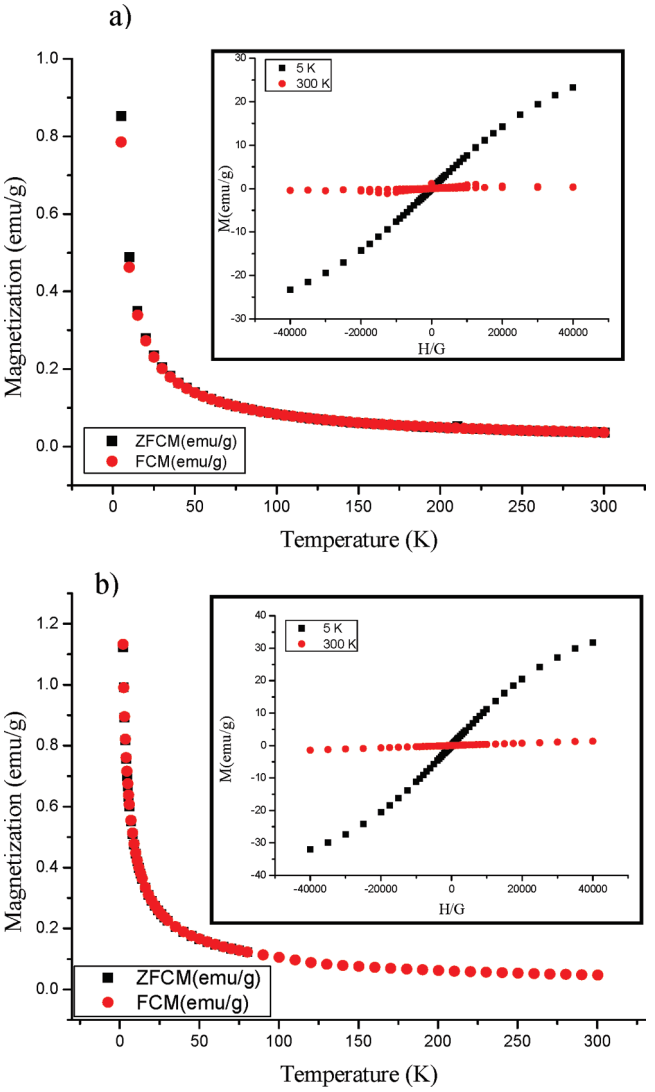

Figure 13. Magnetic measurements of cobalt sulfide thin films deposited from **3** and **4**.

(Figure 13b, inset) and for Co_4S_3 films deposited from complex **5** is 2.1 emu/g. It suggests that the difference in magnetization value of films deposited from complexes **4**, **5**, and **6** due to shape anisotropy would exert a tremendous influence on their magnetic behavior.

Conclusions

Cobalt(III) complexes of 1,1,5,5-tetramethyl [Co{N-(SCNMe$_2$)$_2$}$_3$], 1,1,5,5-tetraethyl-2,4-dithiobiuret [Co{N-(SCNEt$_2$)$_2$}$_3$] and cobalt(II) complex of 1,1,5,5-tetra-*iso*-propyl-2-thiobiuret [Co{N(SOCN^{i}Pr$_2$)$_2$}$_2$] have been synthesized. The X-ray single-crystal structures of complexes **3** and **4** are based on monomer octahedral cobalt(III) atoms, whereas the cobalt(II) in complex **5** is tetrahedral geometry. Thermogravimetric analysis shows all the complexes decompose in a single step to cobalt disulfide. AACVD from complexes **3** and **4** gave $Co_{1-x}S$ films whereas films of Co_3S_4 from **5**. SEM images of the thin films deposited from complex **3** show rodlike morphology, and granular and flowerlike films were deposited from complex **4**, whereas cuboids and stalagmite structures were deposited from complex **5**. TEM images of ground samples for the thin films from complex **3** showed hexagonal nanoplates stacked together to form rods. Similar TEM images from complex **4** gave flower-shaped crystallites composed of hexagonal nanoplates and nanocubes, whereas nanocubes are building blocks for the stalagmite like structures obtained from complex **5**. SAED pattern confirms the single crystalline nature of nanoplates. Magnetic measurements showed the para or ferro-magnetic behavior of the $Co_{1-x}S$ and Co_4S_3 crystallites. The as-deposited films are stable for months in open atmosphere as confirmed by XRD.

Acknowledgment. K.R. is grateful to ORS and The University of Manchester for financial support. The authors also thank EPSRC, U.K., for the grants to P.O.B. that have made this research possible.

Supporting Information Available: Crystallographic information files (CIF) for compounds **1**, **2**, **3**, **4**, and **5**; GC-MS charts (PDF). This material is available free of charge via the Internet at http://pubs.acs.org.